Low-Cost Goethite Nanorods for As (III) and Se (VI) Removal from Water

Mokhtar Ali Amrani [1,2,3,*], **Atef M. Ghaleb** [4], **Adham E. Ragab** [4], **Mohamed Z. Ramadan** [4] **and Tamer M. Khalaf** [4,5]

1 Faculty of Engineering and Information Technology, Taiz University, Taiz 6803, Yemen
2 School of Engineering Sciences and Technology (SEST), University of Hyderabad, Hyderabad 500046, India
3 Faculty of Engineering and Information Technology, Al-Janad University for Science & Technology, Taiz 6813, Yemen
4 Department of Industrial Engineering, College of Engineering, King Saud University, Riyadh 11421, Saudi Arabia; aghaleb@ksu.edu.sa (A.M.G.); aragab@ksu.edu.sa (A.E.R.); mramadan1@ksu.edu.sa (M.Z.R.); tamkhalaf@ksu.edu.sa (T.M.K.)
5 Department of Mechanical Engineering, College of Engineering, Al-Azhar University, Cairo 11371, Egypt
* Correspondence: mokhtar.fe@just.ac; Tel.: +9-67-71618-6473

check for updates

Abstract: Arsenite (As(III)) and Selenate (Se(VI)) are universally touted as extremely toxic oxyanions in natural and industrial water systems. Thus, the production of low-cost adsorbents that are scalable and toxic-free is of great importance today. In this work, a large-scale goethite nanorods (α-*FeOOH* NRs) is synthesized using a modified rapid hydrolysis method. The obtained powder is characterized using different multidisciplinary techniques. Accordingly, the results showed uniform and straight nanorods (length ~400 nm and diameter ~40 nm) resembling cigar-like morphology while the structure is confirmed to be of orthorhombic α-*FeOOH* phase. The potential application of this material to adsorb As (III) and Se (VI) ions in water is explored. In particular, for initial adsorbate concentrations (~500 μg/L), the removal efficiencies are found exceptional with α-*FeOOH* doses of 0.33 g/L and ~0.5 g/L for As (III) and Se (VI), respectively. Attractively, the adsorption capacities were estimated using trusted isotherms and then experimentally verified at ultimately high concentrations. Besides, a pH-controlled adsorption study showed that a pH of 5–8 is a favored range for higher ionic uptake, which meets the World Health Organization (WHO) benchmarks of drinking water. To conclude, the α-*FeOOH* NRs are potential adsorbent for the sustainable removal of toxin ions in water systems.

Keywords: iron oxy-hydroxide; water treatment; water pollution; heavy metals; arsenic; selenium

1. Introduction

The existence of heavy metals in water systems, soils, and sediments is a worldwide health issue [1–3]. Particularly, arsenic and selenium are among the most toxic elements found in natural and industrial environments. They are naturally present in water, soil, rocks, animals, plants, and air [4–8]. Arsenite (As(III)) is an extremely toxic and hazardous substance in groundwater and a difficult pollutant to be removed from water systems [6,7]. Similarly, Selenite (Se(IV)) and Selenate (Se(VI)) are the most commonly present toxic selenium species in the ecosystem [8]. Together, As(III) and Se(VI) ions are highly toxic, mobile, soluble in water, and found in high concentrations in the ground and industrial waters [6–8]. Therefore, their remediation using low-toxicity and low-cost materials is a great challenge [6–8].

Indeed, adsorption is an approved and efficient technology for the remediation of toxic ions in water, owing to its simplicity and applicability at the end user [1,2]. In fact, numerous studies have

suggested various classes of materials and composites at nanoscale for toxic ions' uptake in water [2,3]. However, most suggested adsorbents are unstable in water, release secondary contaminants, show low adsorption capacity and selectivity, and are often difficult to remove from the water. What is more, the bulk production of such adsorbents is challenging, and the economic feasibility is not viable [2].

Iron oxy-hydroxides, owing to their unique chemical structures, high stability, and low toxicity, have shown extraordinary adsorption affinity in water systems [9–11]. Goethite (*α-FeOOH*) is perhaps the most popular and stable iron oxy-hydroxide polymorph that is found in natural soils and sediments, plausibly due to its high thermodynamic stability and high mobility [10–14]. It occupies an open channel structure and extremely high surface activity, which significantly contributes to its adsorption properties [12–14]. Natural and synthesized *α-FeOOH* polymorphs have been extensively studied as an excellent adsorbent for the elimination of hazardous species from aqueous solutions [13–16]. That could be attributed to its outstanding surface properties, high stability, cost-effective, and toxic-free properties [11,12]. Truly, the adsorption properties of goethite are greatly influenced by their unique chemical and physical properties. In particular, the antiferromagnetic nature of goethite [17,18], surface properties [19,20], colloidal stability [19,21], and the temperature at which the adsorption process occurs [22] are important parameters for the uptake of toxic ions by goethite surfaces. The morphology of the goethite also plays a crucial role, affecting the ion removal efficiencies [23]. In view of the above, the *α-FeOOH* phase was widely synthesized by several synthetic methods; among which, precipitation and thermo-hydrolysis methods are the most used processes. The above chemical methods involve extremely slow chemical reactions, in terms of long hours to a few days, low yield production, and often involve the use of unsafe chemicals [10–12]. The present study introduced an approach to the synthesis of bulk and highly crystalline *α-FeOOH* nanorods NRs using a simple and rapid hydrolysis method. Furthermore, the characterization of the obtained nanorods is systematically carried out by using multiple techniques. Laboratory adsorption kinetics, batch, and pH experiments at different conditions are conducted to study the affinity of *α-FeOOH* NRs to adsorb As(III) and Se(VI) ions from water. Surface properties of *α-FeOOH* NRs are correlated to explain their interesting uptake properties and potentials to remove water pollutants.

2. Experimental Work

2.1. Materials and Methods

$FeCl_3$ (98%, Fisher Scientific, Nagpur, India) and NaOH pellets (98%, Fisher Scientific, Nagpur, India) were used as a precursor and reducing agent, respectively. Besides, NaOH was used as the reducing agent as well as hydroxyl ions' generator in the reaction. In a quite simple procedure, 6.49 g of ferric chloride ($FeCl_3$) was dispersed in 200 mL of distilled water in a 2 L glass-beaker. In the next step, the NaOH solution was slowly added under room conditions with continuous control of pH to be ~11. The reaction was then allowed to continue under rapid stirring at 60 °C for 2 h. until the color of the resultant solution changed to a yellowish brown-like color. In the subsequent step, the obtained solution was allowed to precipitate and then filtered using a vacuum filtration system. Finally, the obtained precipitate was repeatedly cleaned up with water, and ethanol and then dried at 60 °C for 6 h. Basically, the plausible reaction is expected to proceed in two steps wherein iron hydroxide (*Fe(OH)₃*) is produced during the first step according to Equation (1):

$$FeCl_3 + NaOH \rightarrow NaCl + Fe(OH)_3 \tag{1}$$
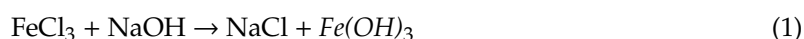
Accordingly, during the second step, *Fe(OH)₃* transforms to oxy-hydroxide (*α-FeOOH*) due to the presence of appropriate hydroxyl ions that could dehydrate hydroxide to the oxy-hydroxide phase. Of course, this reaction involves more oxygen molecules for faster kinetics based on Equation (2).

$$Fe(OH)_3 \rightarrow \alpha\text{-}FeOOH + H_2O \tag{2}$$

In fact, maintaining high alkalinity (here pH is ~11) during the reaction is expected to speed-up the reaction process. However, precise control of the reaction pH is needed to avoid the formation of other phases such as ferrihydrite at higher pH (>12) [24]. Herein, conducting the reaction at pH ~11 for ~2 h was the optimum period for obtaining the goethite phase, which is far less than the required time in other similar synthesis methods to obtain *α-FeOOH* NRs [10–12,24,25]. Interestingly, conducting the experiments in large beakers (here, it was 2 L) diminished the reaction time several folds. Indeed, large beakers provide a proper environment to accelerate the oxygen extraction process from the air that is needed for the growth of the goethite phase. In other words, large beakers offer large contact areas between the air and the solution in the reaction, and therefore rapid reaction occurred. Accordingly, the present study claims that an increase in the beaker size could also cut the reaction time, which opens a novel approach for cost-effective continuous production of scalable *α-FeOOH* NRs in the air-rich environment.

2.2. Adsorption Experiments

A standard stock solution of commercially available Arsenite (As(III)) of 1000 mg/L concentration (Inorganic Ventures, Christiansburg, Virginia, USA) was diluted with distilled water. Se(VI) solutions were prepared by adding appropriate amounts of 1000 mg/L selenate (Inorganic Ventures, Christiansburg, Virginia, USA) to distilled water and used as test solutions. The batch adsorption experiments of As(III) and Se(VI) uptake were designed to analyze the adsorbent dose, kinetics, and effect of pH. Adsorbent dose experiments were performed by adding a different quantity of *α-FeOOH* to As(III) and Se(VI) containing water samples prepared in the lab. As(III) or Se(VI) solution (containing 800 mL water, As(III) 515.34 μg/L and pH ~7) was used for batch experiments. Briefly, 100 mL of As(III) or Se(VI) solution was added to conical flasks. *α-FeOOH* powder in the range of 0.05–1 g/L was dispersed in seven flasks, and one flask was kept as a blank reference. The flasks containing the test solutions with adsorbent were shaken uniformly using a laboratory shaker (Make: Remi) at 150 rpm and at room temperature for 6 h. Adsorption pH study was performed at ~500 μg/L adsorbate ionic concentration, 6 h contact time, and 0.25 g/L goethite dose. The experiments of solution pH were conducted using a pH meter (OAKION, Eutech Instruments), while the variation of solution pH was controlled by using 1 M NaOH or 1 M HCl in the range of 3–12. The measurements were conducted after solutions being shaken for 6 h to attain equilibrium.

Adsorption kinetics study was conducted in a single conical flask with an *α-FeOOH* dose of 0.5 g/L, pH 7.2, and ~500 μg/L of As(III) or Se(VI) concentrations. Adsorption of As(III) and Se(VI) on *α-FeOOH* was monitored as a function of time starting from 1 min to 120 min. Meanwhile, the solution pH was determined by a laboratory pH meter (Make: Thermo). In the final step, samples were filtered using 0.22 μm disposable membrane filters. Finally, the filtered water was analyzed for As(III) and Se(VI) using Inductively Coupled Plasma-Mass Spectroscopy (ICP-MS, Perkin Elmer, NexIon 300X, Waltham, Massachusetts, USA) following standard procedures of sample preparation.

Regeneration experiments are essential for identifying the reusability of an adsorbent. Herein, a modified desorption procedure was conducted by a normal washing process that uses distilled water instead of strong alkaline water. That is to prevent phase transformation. In brief, 100 mL of As(III) or Se(VI) (~8300 μg/L) solution was diluted with 1.0 g/L of *α-FeOOH* adsorbent at pH ~6.7 and room temperature. After equilibration for 3 h, the obtained solution was then allowed to settle down, filtered using centrifugal filtering, and dried at 100 °C for 2 h. in the next step, the filtrate was analyzed for As(III) and Se(VI) ions. The *α-FeOOH* nanorods residues were regenerated by leached out As(III) and Se(VI) ions using only distilled water and then dried at 100 °C for 2 h. Finally, the obtained powder was weighed using an electronic balance and reused again. The above process was repeated five times and the obtained powder was then characterized for identifying its structure and morphology.

3. Results and Discussion

3.1. Structural and Morphological Study

The color (dark yellowish-brown) of the obtained solution and powder (Figure 1) is the first indication of the synthesis of the α-*FeOOH* phase [26]. Besides, the X-ray diffraction (XRD) (D8 Advance X-ray Diffractometer, Bruker, Billerica, Massachusetts, USA) pattern obtained from the as-synthesized sample is displayed in Figure 2a. The diffraction peaks are indexed to the orthorhombic structure phase of α-*FeOOH* (*JCPDS* file No. 81 0463) [27]. The diffractogram revealed the presence of no other diffraction peaks of impurities phases thus suggesting the pure phase synthesis. Of note, the difference in peak broadening indicates the high surface defects and the presence of asymmetry in the crystallite geometries. Accordingly, the average crystallite size of α-*FeOOH* was estimated by Scherrer's formula at ~11.34 nm. Later on, most of these fine crystallites under the van der wall forces get attracted in a certain direction to form rod-like particle features [12].

Figure 1. Photographs of α-*FeOOH*: (**a**) solution; (**b**) powder.
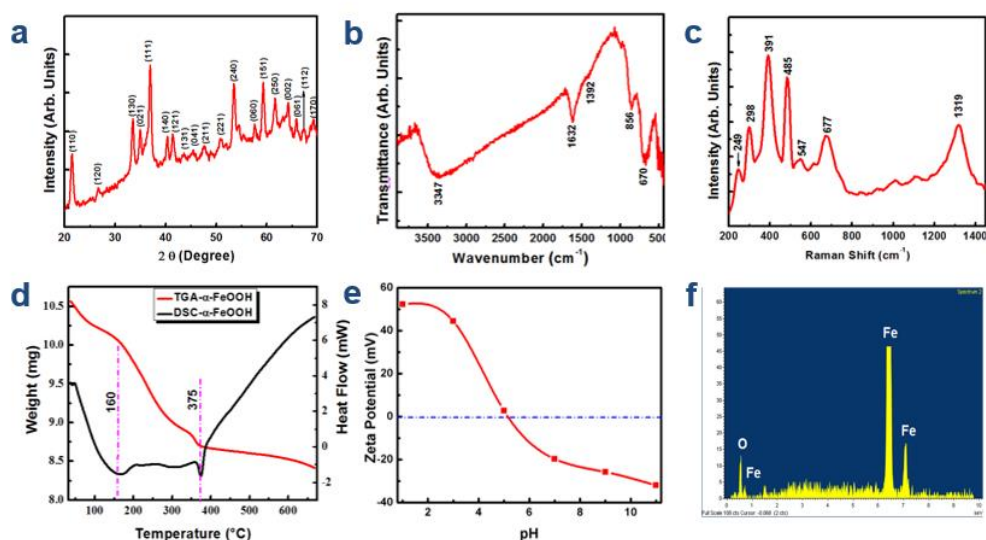
Figure 2. (**a**) X-ray diffraction diagram (XRD); (**b**)Fourier transforms infrared (FTIR) graph; (**c**) Raman spectrum; (**d**) Differential scanning calorimetry (DSC) and thermo-gravimetric analysis (TGA) thermal analysis; (**e**) Zeta potential; (**f**) Energy dispersive spectroscopy (EDS) of α-*FeOOH* nanorods NRs.

Fourier transforms infrared (FTIR) spectrophotometer (Model: Thermo Scientific Nicolet 380, Thermo Fisher Scientific, Waltham, Massachusetts, USA) was used to study the presence of different chemical groups in the sample. The spectrum obtained from the sample is exhibited in Figure 2b.

The band at 670 cm^{-1} is assigned to Fe-O stretching of *α-FeOOH* [28]. The band at 856 cm^{-1} is attributed to the δ-OH in-plane bending of *α-FeOOH* [28]. Also, the peaks at ~1632 and ~1392 cm^{-1} are allocated to the O-H vibrational mode of absorbed H_2O species and structural O-H groups on the surface of *α-FeOOH*, respectively. The prominent peak at 3347 cm^{-1} is related to the vibrational stretching mode of O-H groups attracted to the surface. Of note, the FTIR analysis shows the absence of carboxyl legends, plausibly due to the use of water solvent and not alcoholic solvents.

Raman scattering data was obtained using an Nd-YAG laser (532 nm laser). Figure 2c depicts the Raman spectrum obtained from the sample. In general, it is a powerful characterization tool for those materials with dynamic phase transformation such as iron oxides [11]. Raman bands at ~249, ~298, ~391, ~485, ~520, ~547, and ~677 cm^{-1} in a single sample are specific to the *α-FeOOH* [29,30]. One wide and intense band at 1319 cm^{-1} was attributed to a two-magnon scattering [29].

Figure 2d elucidates TGA-DSC (Thermo-gravimetric analysis-differential scanning calorimetry) profile measurements that provide precise information on the thermal stability of the *α-FeOOH* sample. Thermo-gravimetric analysis (TGA) (Perkin Elmer, Waltham, Massachusetts, USA) is a proper technique to study the dehydration process of iron oxy-hydroxides. It accurately estimates the water weight loss (red curve of Figure 2d) as a function of temperature under inert or reactive atmospheres. Weight loss leads to dynamic changes of crystallization and phase transformation in such an iron oxy-hydroxide phase transform to iron oxide. Besides, it affords valuable information on the chemical reaction and oxidation rate changes as a function of temperature. A considerable weight loss was observed below 150 °C, which can be ascribed to the loss of surface-bonded water molecules and partial endothermic dehydration of iron oxy-hydroxide. However, a sharp loss of water molecules was observed in the 150–375 °C temperature range, attributed to lattice and interlayer water losses [31]. Consequently, a little amount of weight loss was also observed in a wider temperature range of 370–675 °C. This slight loss is attributed to the structural deformation, indicating a complete phase transformation of *α-FeOOH* to *α-Fe₂O₃* at temperature 375 °C. Also, oxidation of the organic and surface residues is represented by exothermic bands at 155 to 370 °C [32]. DSC curve (black curve of Figure 2d) supports the findings of TGA analysis. It shows a similar two critical points. The first transition at 160 °C is due to the endothermic nature of water molecules removal, indicating that this powder contains a large proportion of H_2O molecules, plausibly due to low temperature drying. Likewise, the second transition observed at ~375 °C represents a complete phase transformation to *α-Fe₂O₃* [31,32]. This decomposition temperature is larger than many previous studies, since it is dependent on the particle size and morphology. In other words, nanosize particles of *α-FeOOH* are thermally more stable than larger particles [10].

Zeta potential experiment (Nanoparticle analyzer, Horiba Scientific, Minami-ku, Kyoto Japan) was conducted using a light scattering method by a zeta analyzer. Figure 2e shows a typical representation of surface charge density that is commonly used to evaluate the dispersion of nanoparticles at varied pH. In fact, this is a commonly used procedure to present the surface charge observations in an attempt to study the interactions between the particles and their aqueous surroundings, and therefore their stability as well. The point of zero charges (PZC) was measured to be at pH 5.2. However, the results implied that zeta potential, in general, has relatively low magnitude values with a range of 52 mV at lower pH and −32 mV at higher pH values. Indeed, the lower the value of PZC, the weaker is the repulsive force (higher attractive forces) between particles, and therefore aggregation of the particles is plausibly the feasible phenomenon [19]. Accordingly, an evident decrease in the specific surface area in contact with pollutant ions leading to a decrease in As and Se removal. *α-FeOOH* NRs have an affinity to aggregation at different conditions, which in turn affects its interactions with the surface contaminants [19]. At certain pH, the hydroxyl ions are deprotonated, resulting in a negative surface charge (exothermic at room temperature on *α-FeOOH* NRs. These exothermic surfaces of *α-FeOOH* were experimentally verified for As(III) and Se(VI) oxyanions and the results showed weaker interaction even with the increase in solution temperatures [33,34]. At these conditions, the interaction forces get weaker and the adsorption sites are occupied by hydroxyl ions. Therefore,

adsorption is significantly decreased at these pH values. Finally, Figure 2f depicts the energy dispersive spectroscopy (EDS) measurements. The results show that iron and oxygen molecules are the only constituents of the powder indicating that no other contaminants in the powder and thus the purity of *α-FeOOH* polymorph.

Figure 3 shows the morphological and structural characterization of *α-FeOOH*. Particularly, Figure 3a displays plane view field emission scanning electron microscope (FE-SEM, Zeiss ultra 55) micrograph of bulk *α-FeOOH* NRs, clearly depicting the uniform nanorods. Of note, the micrograph shows very small spherical-shaped particles attached to the nanorods with typical dimensions of ~10 nm. These observations correlate well with crystallite size calculated from the XRD diffractogram. Furthermore, the systematic growth of *α-FeOOH* NRs could be ascribed to the formation of O-H groups that is responsible for electron diffusion and then the plausible growth of small clusters. Of course, these clusters, in the absence of surfactants, grow in a particular surface to form 1-D *α-FeOOH* NRs due to the highly attractive forces among the particles. Certainly, the uniformity of the nanorods is directly proportional to the uniform distribution of OH species in the solution (no local gradient of pH). Likewise, the Transmission electron microscope (TEM, FEI TECNAI G2) micrograph (Figure 3b,c) shows a uniform and straight nanorods resembling a cigar-like feature of ~50 nm diameter and ~400 nm length. The above dimensions correlate well with the obtained from the scanning electron microscopy (SEM) image. Finally, Figure 3d depicts the SAED pattern obtained from the nanorods. Indeed, the pattern shown in bright dots indicates a single crystalline structure of *α-FeOOH* NRs. Obviously, the pattern is identified in two orthogonal directions (010) and (200) of the goethite structure, which is marked by inclined and perpendicular dotted lines [19], as shown in Figure 3d. Observably, the uniform distribution of the bright dots is an indication of the pure phase of *α-FeOOH* [19]. To conclude, it can be inferred that the grown *α-FeOOH* NRs are single crystalline structure and of a single pure phase.
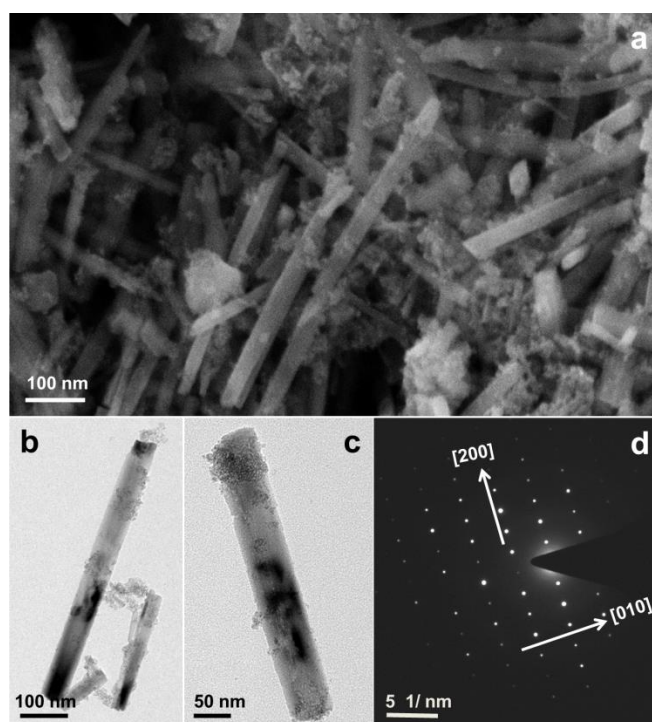
Figure 3. Plane view (**a**) Scanning electron microscope (SEM) micrograph; (**b**) and (**c**) Transmission electron microscope (TEM) micrographs; (**d**) Electron diffraction pattern of *α-FeOOH* NRs (water was used as a solvent).

3.2. Adsorption Experiments of As(III) and Se(VI)

The analysis of FTIR (Figure 2b) displayed functionalized surfaces while XRD results (Figure 2a) expressed the channel-like structure. In contrast, the analysis of PZC revealed exothermic surfaces and low adsorbent-adsorbate attraction forces suggesting weak and slow adsorption, which is a common phenomenon for goethite [33–35]. However, the nano-sized rods could provide a large surface area in contact with adsorbate ions. This evidence is fundamental for strong binding ligand uptake and substitutions with As(III) and Se(VI) ions. Furthermore, adsorption isotherms were implemented to eventually explain the nature of adsorbent-adsorbate physiochemical interactions. Of note, the base lines of heavy metal intensity were selected for As and Se, as per the WHO standards of drinking water at 10 and 40 µg/L, respectively. What's more, the removal efficiency (Removal (%)) was employed to present the adsorption data of goethite adsorbent according to Equation (3).

$$Removal\ (\%) = \frac{(C_o - C_e)}{C_o} \times 100\% \tag{3}$$

where C_o and C_e (µg/L or ppb) are the initial and equilibrium concentration of As(III) or Se(VI) in aqueous solution, respectively.

3.2.1. Adsorbent Dose Optimization Study

Figure 4 shows the dose study results and the corresponding Langmuir and Freundlich adsorption isotherms for both As(III) and Se(VI) uptake. Figure 4a,d depict the adsorbent dose data pertaining to As(III) and Se(VI) removal by the *α-FeOOH* adsorbent, respectively. Of course, the adsorbent doses were plotted against the removal efficiency (%) at ~500 µg/L of adsorbate concentrations. As expected, the results revealed a noticeable increase in the removal efficiency as the adsorbent (*α-FeOOH*) dose also increased until a plateau was reached. This stability is presented in a horizontal line as an indication of complete adsorption, whatever the adsorbent dose is. Particularly, the results in the case of As(III) indicate that 0.33 g/L is the optimum dose of *α-FeOOH* adsorbent to remove As(III) ions (~515 µg/L) below the WHO standards (10 µg/L). Results for Se(VI) suggest slightly inferior removal efficiencies and an adsorbent dose of ~0.5 g/L of *α-FeOOH* was sufficient to remove Se(VI) ions (502 µg/L) below the WHO standards (40 µg/L). In fact, among all other phases of selenium oxyanions, Se(VI) often shows slightly lower uptake [35]. Of course, complete adsorption of Se(VI) species and reaching the plateau could be launched at 1.5 g/L of *α-FeOOH* adsorbent, as suggested by the results of Figure 4d. For 1 g/L of *α-FeOOH* dose, 99.7% and 97% removal efficiency was observed for As(III) and Se(VI), respectively. This indicates stronger adsorption affinity between *α-FeOOH* adsorbent surfaces for both As(III) and Se(VI) ions in an aqueous medium, and also using higher than the commonly observed concentrations of these polluting ions.

Adsorption isotherms are implemented mainly to estimate the maximum adsorption capacity of *α-FeOOH* NRs and to investigate the adsorption mechanism of As(III) and Se(VI) oxyanions by *α-FeOOH*. Accordingly, well known adsorption models (Langmuir and Freundlich) were implemented to fit the equilibrium dose data of *α-FeOOH* adsorbent against As(III) and Se(VI) adsorbate ions in water systems. Basically, adsorption isotherms elucidate the nature of adsorbate diffusion to the adsorbent at conditions quite similar to those relevant for practical conditions for the removal of these pollutants. In particular, Langmuir isotherm is described by linear Equation (4).

$$\frac{1}{q} = \frac{1}{Q_{\max}} + \frac{1}{K_l \cdot Q_{\max}} \left(\frac{1}{C_e}\right) \tag{4}$$

where $b = \frac{1}{Q_{max}}$ and $a = \frac{1}{K \cdot Q_{max}}$ are Langmuir constants that can be calculated based on the intercept and slope of Langmuir isotherm plot as shown in Figure 4b,e for As(III) and Se(VI), respectively.
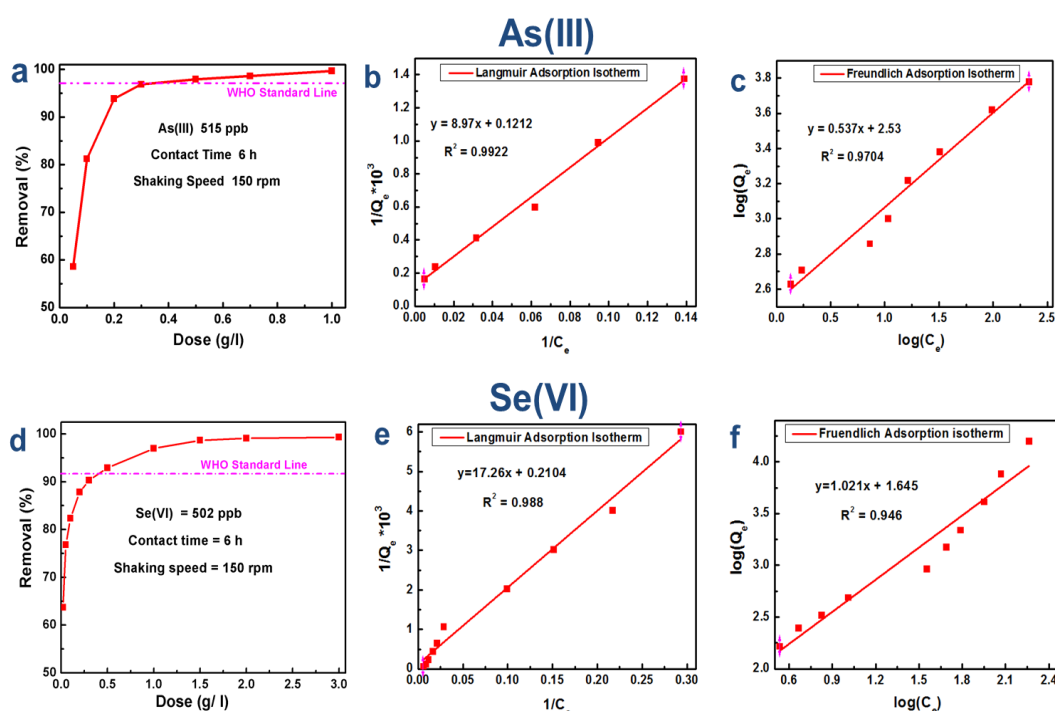
Figure 4. Illustration graphs of (**a**,**d**) batch study, (**b**,**e**) Langmuir, and (**c**,**f**) Freundlich adsorption isotherms pertaining to As(III) and Se(VI) removal by *α-FeOOH* NRs, respectively. WHO standard line for the concentration of these ions was plotted for reference.

The maximum adsorption capacities (Q_{max}) of *α-FeOOH* adsorbent are determined from the Langmuir model and recorded in Table 1. Particularly, the Q_{max} is found at 8.253 mg/g for As(III), which is higher than most of the reported values [36–38]. However, for Se(VI), the maximum adsorption capacity was 4.753 mg/g, which is also higher than different other synthetic and natural adsorbents as tabulated by Zelmanov and Semiat [39]. These values correlate well with removal efficiencies observed in Figure 4a,d by using Equation (1). Of note, the very high adsorption capacity of *α-FeOOH* is a distinct advantage in addition to its low cost, low toxicity, and present facile synthesis, which can make the present *α-FeOOH* material one of the highest potential adsorbents explored, especially for the As(III) and also for Se(VI) removal. Another indication of good adsorption is the values of the equilibrium parameter (R_L) that are recorded in Table 1. The value of R_L is determined by Equation (5).

$$R_l = \frac{1}{1 + K_l C_o} \tag{5}$$

where K_L and C_o are constants related to the Langmuir model. Calling back the adsorption parameters obtained from Langmuir adsorption isotherm plots, R_L values for As(III) and Se(VI) are found at $R_L = 0.126$ and $R_L = 0.14$, respectively. In general, adsorption is favored when R_l the value is in the 0–1 range. In the present analysis, R_L of both adsorbate oxyanions indicates a favorable monolayer adsorption process, but it also indicates strong adsorption for As(III) than Se(VI). These findings are also confirmed by the correlation coefficient, R^2, from the plots of Figure 4b,e.

In the same way, Freundlich isotherm is another precise adsorption model to describe the interaction mechanism. Of course, if the data fitted well with this isotherm, it indicates heterogeneous adsorption. It gives proper information on the nature of adsorption as well as specific adsorption capacity of the *α-FeOOH*. A linear logarithmic equation of Freundlich isotherm is described in Equation (6).

$$\log(q) = \log(K_f) + n \log(C_e) \tag{6}$$

where n and K_f are constants that could be obtained from the slope and intercept of Freundlich isotherm plots of Figure 4c,f for As(III) and Se(VI), respectively. Specifically, K_f is the specific adsorption capacity and determined using Equation (4) for As(III) and Se(VI) to be 12.52 mg/g and 5.19 mg/g, respectively. Remarkably, the specific adsorption capacities calculated by Freundlich adsorption isotherm also show a lower adsorption affinity for Se(VI) as compared to As(III). Besides, the parameter, n, a dimensionless parameter, indicates the nature and mechanism of adsorption. The values of n as calculated from Freundlich isotherm were 0.537 and 1.017 for As(III) and Se(VI), respectively. Of course, $n < 1$ indicates a strong adsorption affinity. These values, therefore, indicate that As(III) adsorption to *α-FeOOH* surfaces also follows Freundlich isotherm, but Se(VI) does not follow Freundlich isotherm. All in all, by considering the values of R^2, in Table 1 and Figure 4, there is evidence that the adsorption of As(III) and Se(VI) follows Langmuir isotherm, which suggests monolayer adsorption and uniformly distributed adsorption sites on the nanorods surfaces. Also, *α-FeOOH* adsorbent shows more affinity towards As(III) than Se(VI), plausibly due to the electronic properties of both pollutants and the oxidation state [34,35].

Table 1. A representation of Langmuir and Freundlich adsorption isotherms data of the *α-FeOOH* adsorbent for the uptake of As(III) and Se(VI) from water solutions.

| Langmuir Adsorption Isotherm			Freundlich Adsorption Isotherm		
Parameter	As(III)	Se(VI)	Parameter	As(III)	Se(VI)
R^2	0.992	0.989	R^2	0.97	0.946
Q_{max} (mg/g)	8.251	4.753	K_f	12.52	5.19
R_L	0.126	0.14	n	0.537	1.021

3.2.2. Adsorption Kinetics

Figure 5 depicts the adsorption kinetic data and adsorption kinetic isotherms. In view of the above discussion pertaining to adsorption batch and isotherms, the adsorption process was tailored well with Langmuir adsorption isotherm. Besides, the Q_{max} was calculated for As(III) and Se(VI) to be 8.253 and 4.75 mg/g, respectively. To prove these findings experimentally, kinetic studies at extremely high As(III) and Se(VI) test concentrations (~8.3 mg/L) with respect to contact time were conducted. The results of adsorption kinetic studies are plotted in Figure 5a,d. The results implied a rapid uptake (only 1 h) in spite of high dilutions, which is an adequate time to remove As(III) and Se(VI) from the water below WHO standards stipulated for drinking water. Besides, it can be demonstrated that most of the adsorption process took place in the first 1 h in which a plateau was reached with high removal percentage. Specifically, within 3 h contact time, the removal efficiencies reached ~98% and ~80% for As(III) and Se(VI), respectively. However, within 24 h contact time, the removal efficiencies were recorded at ~99.4% and ~84.5% for As(III) and Se(VI), respectively. These results indicate that As(III) ions were completely removed below the WHO standards for drinking water at 8300 μg/L initial dilution. However, ~85% of Se(VI) ions were only adsorbed. Recalling the Q_{max} of *α-FeOOH* adsorbent estimated by Langmuir isotherm of As(III) ($Q_{max} = 8.25$ mg/g) and Se(VI) ($Q_{max} = 4.75$ mg/g); this kinetic study at high concentrations proves experimentally the values of Q_{max} estimated by Langmuir isotherm.

The experimental kinetic data observed from the kinetic study of high arsenic concentration were fitted into pseudo-first-order and pseudo-second-order isotherms. Initially, Pseudo-first-order kinetic isotherm is displayed in Figure 5b,e for As(III) and Se(VI), respectively. The linear form was represented by Equation (7):

$$\log(Q_e - Q_t) = \log(Q_e) - K_1 d_t \tag{7}$$

where Q_t is the adsorbed oxyanions in mg/g at time t while K_1 is the equilibrium rate constant of pseudo-first-order adsorption. Basically, the linearized graphs of $\log(q_e - q_t)$ vs. time (t) gives the rate

constants. Obviously, the results obtained from the figures indicate that the adsorption mechanism does not fit with this model.
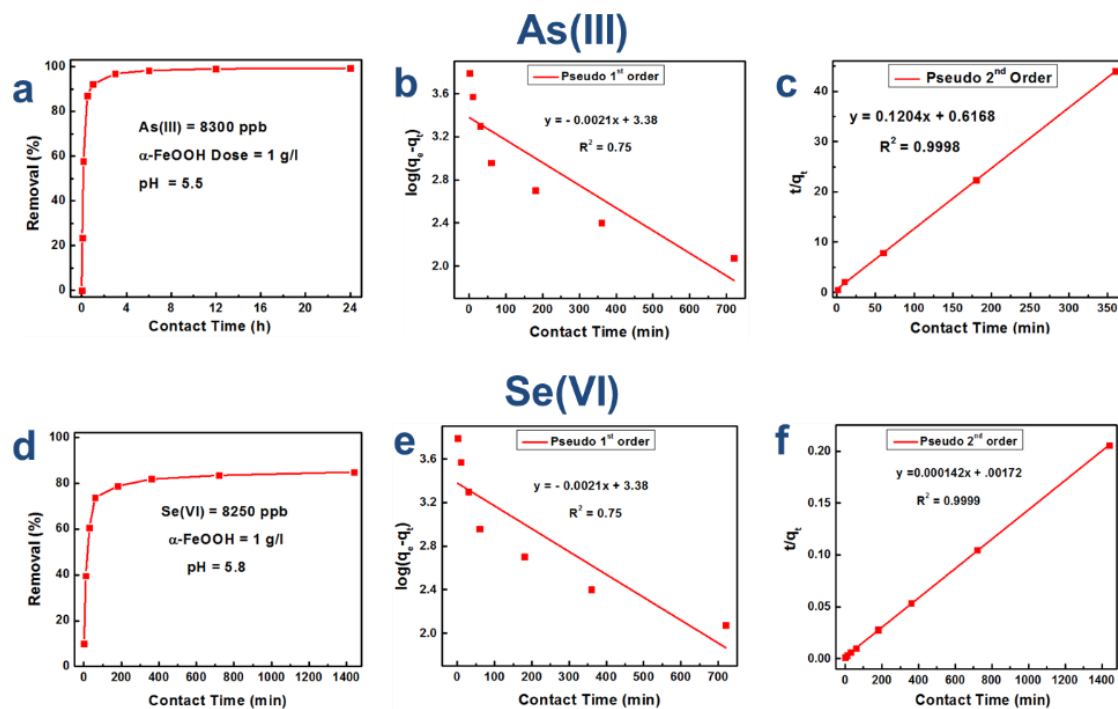
Figure 5. (**a**,**d**) kinetics study data with removal (%) as a function of contact time for *α-FeOOH* adsorbent at high As(III) and Se(VI) concentrations; (**b**,**e**) Pseudo 1st order; and (**c**,**f**) Pseudo 2nd order for As(III) and Se(VI), respectively.

Figure 5c,f represents Pseudo-second-order plots of As(III) and Se(VI), respectively. In general, it describes the physiochemical interaction and migration of adsorbate oxyanions to the adsorbent sites. In other words, chemical bonding and functional groups are responsible for the As(III) and Se(VI) uptake. Notably, the very high values of (R^2) of this model recommend its use to identify the adsorption kinetics. In fact, Pseudo-second-order isotherm usually plotted in its linear form based on Equation (8).

$$\frac{t}{q} = \frac{1}{k_2.q_e^2} + \frac{1}{q_e}t \tag{8}$$

where K_2 is a sorption rate constant measured by g/(mg·min) units. For As(III) experiments (Figure 5c), the results of the Pseudo-second-order model are recorded in Table 2. The results implied that the experimental adsorption capacity is q_e = 8.305 and k_2 = 0.0235, which is almost similar to that calculated by Langmuir adsorption isotherm. This is experimental evidence for the effective adsorption of As(III) by *α-FeOOH* NRs. Similarly, the pseudo-second-order adsorption model of Se(VI) is fitted well and plotted in Figure 5f. The calculated results are tabulated in Table 2, which imply that Q_e = 7.04 and K_2 = 0.01173. In this case, the value of Q_e is relatively higher than Qmax calculated by Langmuir isotherm in Figure 4e. In this way, the kinetics of As(III) and Se(VI) adsorption on *α-FeOOH* NRs surfaces follow pseudo-second-order sorption isotherm, which indicates the chemical nature of adsorption [40]. For Se(VI), the adsorption mechanism fits well with Langmuir isotherms, indicating a chemical interaction. These findings are consistent with the theoretical finding that assumes a mixture of inner- and outer-shell surfaces on *α-FeOOH* [35,41].

Table 2. A representation of kinetic parameters of pseudo-first-order and pseudo-second-order models of the *α-FeOOH* adsorbent for the removal of As(III) and Se(VI) from water.

Pseudo-first-order Isotherm			Pseudo-second-order Isotherm		
Parameter	**As(III)**	**Se(VI)**	**Parameter**	**As(III)**	**Se(VI)**
R^2	0.798	0.75	R^2	0.9485	0.987
q_e	1.48	29.42	q_e	8.302	7.04
K_1	0.005	0.0021	K_2	0.0235	0.012

Figure 6a displays the results of As(III) and Se(VI) adsorption into the surface of *α-FeOOH* NRs with variable pH values. Of note, the experiments were performed at ~500 µg/L adsorbate dilution, 0.25 g/L *α-FeOOH* dose, and 6 h contact time. Apparently, the results demonstrated that adsorption is highly influenced by pH changes. Besides, the results confirmed that the migration of As(III) oxyanions into the negatively charged *α-FeOOH* surfaces is higher and slightly flatter than Se(VI), but selenium adsorption, in general, shows the minimum pH deviation especially at acidic solutions. Of course, the above finding is useful for practical considerations.
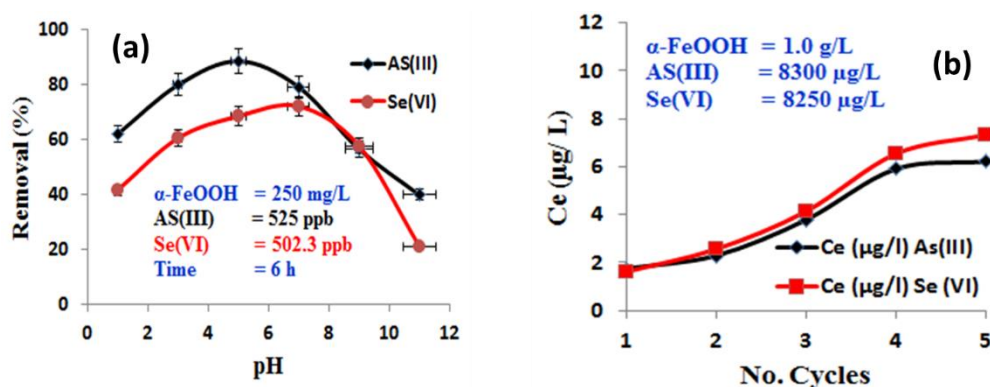
Figure 6. (**a**) pH adsorption study and (**b**) five cycles regeneration experiments of As(III) and Se(VI) ions on the surface of *α-FeOOH* NRs.

Apparently, the results demonstrated that adsorption is highly influenced by pH changes. Besides, the As(III) adsorption is indeed greater than the selenium uptake; however, the swings in ion removal caused by pH variations seem to be similar for both compounds (~50% change between the highest and lowest removal values at different solution pH) [42]. Of course, the above finding is useful for practical considerations.

Figure 6b shows the reuse capability experiment results, which reveal that *α-FeOOH* can be used as an adsorbent for more than five cycles effectively. The experiments considered the amount of adsorbent loss due to the washing and filtration processes in each cycle. The results showed that, in the first cycle, the weight loss of adsorbent was 8.32% and it reduced until it reached 3.87% after the fifth cycle. Therefore, the weight of the powder was measured immediately after each cycle and the quantity of treated water is modified to be equivalent to the weight of the obtained powder after calculating the losses in each reuse. The results indicate a negligible amount of As(III) and Se(VI) ions after each cycle with a slight increase as the number of cycles increases. All in all, the regeneration results implied that the *α-FeOOH* nanorods are an efficient adsorbent for real applications. The capability of several times efficient regeneration enhances the economic feasibility to fabricate real adsorbents based on *α-FeOOH* NRs. Furthermore, easy processing and low-cost iron precursors support its cost-effective production.

Recalling the results of zeta potential experiments from Figure 2e, which suggested that PZC was depicted at pH ~5.2, the ultimate As(III) removal (~92%) was also observed at pH ~5.2 as shown in Figure 6. At pH greater than PZC (pH 5–8) and due to the negatively charged goethite surfaces, the attraction forces get reduced and then lower adsorption of As(III) ions. However, removal is

significantly reduced for the alkaline range 8–12. This large reduction is attributed to the presence of larger concentrations of O-H ions, which compete for arsenic ions to occupy the adsorption sites. Besides, well-fitting to the pseudo-second-order model and Langmuir isotherm suggests chemisorption interaction. Similarly, Se(VI) shows the highest removal efficiency of ~75% at neutral pH 7 but it shows better sorption properties in acidic solution than alkaline solutions. The low removal percentage in pH study could be ascribed to the use of lower *α-FeOOH* doses (0.25 g/L). To conclude, the results implied that the adsorption attraction at an alkaline solution (pH > 7) is unfavorable for As(III) and Se(VI), for the reasons explained above. Similarly, at higher acidic solutions (pH < 3), the removal efficiency of As(III) and Se(VI) on *α-FeOOH* NRs surfaces are also unfavorable. As a conclusion, the removal of As(III) and Se(VI) on *α-FeOOH* surfaces are preferred in the pH range of 5–8. This pH range is consistent with the acceptable pH range (5.5–8) of the drinking water.

Unlike selenite (Se(IV)), which is extensively studied in the literature, the mechanism of adsorption of selenate (Se(VI)) to the surface of goethite is still unclear [35,43–45]. An earlier study by Balistrieri et al. [45], inferred that the adsorption affinity of Se(VI) is much less than selenite anions at all pH values. Furthermore, they found that selenite adsorbs more strongly than selenate at all conditions, plausibly due to the high mobility of selenate. Few studies have investigated the adsorption mechanism of selenate into goethite. However, their conditions were limited to the near-neutral pH [44]. The effect of pH on the adsorption of selenate to the goethite adsorbent has been well studied in the literature [39,41,46–48]. Unlike selenite (Se(IV)), sorption that forms an inner-sphere surface complex selenate behaves in a different way. The interaction mechanism varies with the pH fluctuation and ion strength. In other words, selenate sorption on goethite forms inner-sphere complexes at acidic pH and outer-sphere complexes at alkaline pH. This variation in adsorption with pH could be attributed to the surface charge variation with pH and the predominance of the $HSeO_4^-$ selenium species [39].

To confirm the ionic sorption of As(III) and Se(VI) to the surface of goethite nanorods and to prove their structure after sorption experiments, X-ray diffractograms post to the sorption experiments were conducted. Figure 7 depicts the diffractograms of regenerated goethite nanopowder after five reuse cycles. The peaks indicate that the goethite phase kept unchanged despite the varied intensities and peak shifts toward the right angle in the case of As(III) sample. The observed shift in both cases could be attributed to the semiconducting properties of arsenic and selenium ions. This phenomenon was also observed for selenium in lepidocrite [49].
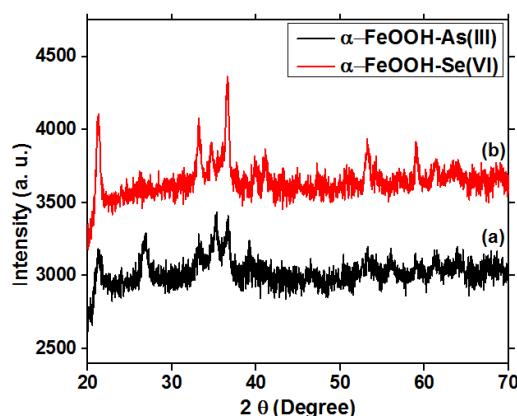

Figure 7. X-ray diffractograms of *α-FeOOH* nanorods after regeneration experiments.

4. Conclusions

Uniform *α-FeOOH* NRs resembling cigar-like nanostructures (~40 nm diameters) were synthesized by a simple hydrolysis method that does not use any toxic chemicals. The proposed synthesis method is easy, rapid, and scalable. The phase structure of *α-FeOOH* was verified by XRD, SAED, and Raman spectroscopy. Also, surface properties of *α-FeOOH* were studied by FTIR and zeta potential

measurements as a function of pH and found that the zero charges point was observed at pH_{pzc} = 5.2. The obtained *α-FeOOH* NRs was used as an efficient adsorbent for As(III) and Se(VI) from water. The analysis of the dose study shows that 0.4 g/L of *α-FeOOH* NRs are an optimum dose for the removal of ~500 μg/L of As(III) and Se(VI). Additionally, *α-FeOOH* NRs exhibited rapid adsorption kinetics in less than 1 h even at higher dilution (8300 μg/L). The maximum adsorption capacities of *α-FeOOH* adsorbent (which is calculated using Langmuir isotherm) for As(III) and Se(VI) were estimated at 8.23 and 4.75 mg/g, respectively. The adsorption capacity of *α-FeOOH* (Dose 1 g/L) was experimentally verified by performing kinetic experiments at As(III) and Se(VI) concentrations of ~8300 μg/L and the results showed 99.3% and 84% removal in 1 h contact time, respectively. The adsorption measurements elucidated that the adsorption of As(III) and Se(VI) to the *α-FeOOH* NRs is rapid and monolayer in nature. Finally, *α-FeOOH* polymorph is a potential excellent adsorbent owing to its scalable and easy synthesis, insolubility in water, low-toxicity, and cost-effective material.

Author Contributions: Conceptualization, M.A.A., M.Z.R.; data curation, M.A.A., T.M.K.; formal analysis, M.A.A. and A.M.G., A.E.R.; investigation, M.A.A., A.E.R.; methodology, M.A.A., A.E.R.; resources, M.A.A., M.Z.R.; software, M.A.A., A.M.G., M.Z.R.; supervision, M.A.A.; validation, M.A.A.,T.M.K.; visualization, M.A.A.,A.M.G., M.Z.R., T.M.K.; writing—original draft, M.A.A. and A.M.G.; writing—review and editing, A.E.R., M.Z.R., T.M.K. All authors have read and agreed to the published version of the manuscript.

Conflicts of Interest: There are no conflicts of interest to disclose.

References

1. Shannon, M.A.; Bohn, P.W.; Elimelech, M.; Georgiadis, J.G.; Marinas, B.J.; Mayes, A.M. Science and technology for water purification in the coming decades. *Nature* **2008**, *452*, 301–310. [CrossRef]
2. Lorenzo, T.D.; Hose, G.C.; Galassi, D.M.P. Assessment of Different Contaminants in Freshwater: Origin, Fate, and Ecological Impact. *Water* **2020**, *12*, 1810. [CrossRef]
3. Jawed, A.; Saxena, V.; Pandey, L.M. Engineered nanomaterials and their surface functionalization for the removal of heavy metals: A review. *J. Water Process Eng.* **2020**, *33*, 101009. [CrossRef]
4. Mandal, B.K.; Suzuki, K.T. Arsenic around the world: A review. *Talanta* **2002**, *58*, 201–235. [CrossRef]
5. Conde, J.E.; Alaejos, M.S. Selenium Concentrations in Natural and Environmental Waters. *Chem. Rev.* **1997**, *97*, 1979–2004. [CrossRef]
6. Lata, S.; Samadder, S.R. Removal of arsenic from water using nano adsorbents and challenges: A review. *J. Environ. Manag.* **2016**, *16615*, 387–406. [CrossRef]
7. Siddiqui, S.I.; Chaudhry, S.A. Iron oxide and its modified forms as an adsorbent for arsenic removal: A comprehensive recent advancement. *Process Saf. Environ. Prot.* **2017**, *111*, 592–626. [CrossRef]
8. Yigit, N.O.; Tozum, S. Removal of selenium species from waters using various surface-modified natural particles and waste materials. *Clean* **2012**, *40*, 735–745. [CrossRef]
9. Casentini, B.; Lazzazzara, M.; Amalfitano, S.; Salvatori, R.; Guglietta, D.; Daniele Passeri, D.; Belardi, G.; Trapasso, F. Mining Rock Wastes for Water Treatment: Potential Reuse of Fe-and Mn-Rich Materials for Arsenic Removal. *Water* **2019**, *11*, 1897. [CrossRef]
10. Navrotsky, A.; Mazeina, L.; Majzlan, J. Size-driven structural and thermodynamic complexity in iron oxides. *Science* **2008**, *319*, 1635–1642. [CrossRef]
11. Cornell, R.M.; Schwertmann, U. *The Iron Oxides*, 2nd ed.; Wiley VCH-Verlag Publishers: New York, NY, USA, 2003.
12. Xu, G.; Yang, X.; Spinosa, L. Development of sludge-based adsorbents: Preparation, characterization, utilization and its feasibility assessment. *J. Environ. Manag.* **2015**, *151*, 221–232. [CrossRef] [PubMed]
13. Liu, H.; Chen, T.; Frost, R.L. An overview of the role of goethite surfaces in the environment. *Chemosphere* **2014**, *103*, 1–11. [CrossRef] [PubMed]
14. Jaiswal, A.; Banerjee, S.; Mani, R.; Chattopadhyaya, M.C. Synthesis, characterization and application of goethite mineral as an adsorbent. *J. Environ. Chem. Eng.* **2013**, *1*, 281–290. [CrossRef]

15. Kumar, E.; Bhatnagar, A.; Hogland, W.; Marques, M.; Sillanpää, M. Interaction of inorganic anions with iron-mineral adsorbents in aqueous media-A review. *Adv. Colloid. Interf. Sci.* **2014**, *203*, 11–21. [CrossRef] [PubMed]

16. Velimirovic, M.; Bianco, C.; Ferrantello, N.; Tosco, T.; Casasso, A.; Sethi, R.; Schmid, D.; Wagner, S.; Miyajima, K.; Klaas, N.; et al. A Large-Scale 3D Study on Transport of Humic Acid-Coated Goethite Nanoparticles for Aquifer Remediation. *Water* **2020**, *12*, 1207. [CrossRef]

17. Kim, J.; Nielsen, U.G.; Grey, C.P. Local Environments and Lithium Adsorption on the Iron Oxyhydroxides Lepidocrocite (ç-FeOOH) and Goethite (r-FeOOH): A 2H and 7Li Solid-State MAS NMR Study. *J. Am. Chem. Soc.* **2008**, *130*, 1285–1295. [CrossRef]

18. Llavona, A.; Prados, A.; Velasco, V.; Crespo, P.; Sanchez, M.C.; Perez, L. Electrochemical synthesis and magnetic properties of goethite single crystal nanowires. *Cryst. Eng. Comm.* **2013**, *15*, 4905–4909. [CrossRef]

19. Stemig, A.M.; Do, T.A.; Yuwono, V.M.; Arnold, W.A.; Penn, R.L. Goethite nanoparticle aggregation: Effects of buffers, metal ions, and 4-chloronitrobenzene reduction. *Environ. Sci.* **2014**, *1*, 478–487. [CrossRef]

20. Gimenez, J.; Martınez, M.; de Pablo, J.; Rovira, M.; Duroc, L. Arsenic sorption onto natural hematite, magnetite, and goethite. *J. Hazard. Mater.* **2007**, *141*, 575–580. [CrossRef]

21. Fernando, S.; Baynes, M.; Chen, B.; Banfield, J.F.; Zhang, H. Compressibility and structural stability of nanoparticulate goethite. *RSC Adv.* **2012**, *2*, 6768–6772. [CrossRef]

22. Hao, L.; Ouyang, T.; Lai, L.; Liu, Y.X.; Chen, S.; Hu, H.; Chang, C.T.; Wang, J.J. Temperature effects on arsenate adsorption onto goethite and its preliminary application to arsenate removal from simulative geothermal water. *RSC Adv.* **2014**, *4*, 51984–51990. [CrossRef]

23. Ghosh, M.K.; Poinern, G.E.J.; Issa, T.B.; Singh, P. Arsenic adsorption on goethite nanoparticles produced through hydrazine sulfate assisted synthesis method. *Korean J. Chem Eng.* **2012**, *29*, 95–102. [CrossRef]

24. Enlei, Z.; Guosheng, W.; Xiaozhu, L.; Zhumin, W. Synthesis and influence of alkaline concentration on α-FeOOH nanorods shapes. *Bull. Mater. Sci.* **2014**, *37*, 761–765.

25. Mohapatra, M.; Gupta, S.; Satpati, B.; Anand, S.; Mishra, B.K. PH and temperature dependent facile precipitation of nano-goethite particles in Fe(NO$_3$)$_3$–NaOH–NH$_3$NH$_2$HSO$_4$–H$_2$O medium. *Coll. Surf. A Physicochemical. Eng. Aspects* **2010**, *355*, 53–60. [CrossRef]

26. Scheinost, A.C.; Schwertmann, U. Color identification of iron oxides and hydroxysulfates-Use and limitations. *Soil Sci. Soc. Am. J.* **1999**, *63*, 1463–1471. [CrossRef]

27. Jia, X.H.; Song, H.J. Facile synthesis of monodispersed a-Fe$_2$O$_3$ Microspheres through template-free hydrothermal route. *J. Nanopart Res.* **2012**, *14*, 663–670. [CrossRef]

28. Maiti, D.; Manju, U.; Velaga, S.; Devi, P.S. Phase Evolution and Growth of Iron Oxide Nanoparticles: Effect of Hydrazine Addition During Sonication. *Cryst. Growth Design* **2013**, *13*, 3637–3644. [CrossRef]

29. Bellot-Gurlet, L.; Neff, D.; Réguer, S.; Monnier, J.; Saheb, M.; Dillmann, P. Raman Studies of Corrosion Layers Formed on Archaeological Irons in Various Media. *J. Nano. Res.* **2009**, *8*, 147–156. [CrossRef]

30. Hanesch, M. Raman spectroscopy of iron oxides and (oxy)hydroxides at low laser power and possible applications in environmental magnetic studies. *Geophys. J. Int.* **2009**, *177*, 941–948. [CrossRef]

31. Gialanella, S.; Girardi, F.; Ischia, G.; Lonardelli, I.; Mattarelli, M.; Montagna, M. On the goethite to hematite phase transformation. *J. Therm. Anal. Calorim.* **2010**, *102*, 867–873. [CrossRef]

32. Guo, H.; Barnard, A.S. Thermodynamic modelling of nanomorphologies of hematite and goethite. *J. Mater. Chem.* **2011**, *21*, 11566–11577. [CrossRef]

33. Vlasova, N.N.; Kersten, M. Effect of Temperature on Selenate Adsorption by goethite. In *Water-Rock Interaction Book*; Taylor & Francis: Abidgon, UK, 2010; pp. 693–696.

34. Kersten, M.; Vlasova, N. Arsenite adsorption on goethite at elevated temperatures. *Appl. Geochem.* **2009**, *24*, 32–43. [CrossRef]

35. Das, S.; Hendry, M.J.; Essilfie-Dughan, J. Adsorption of selenate onto ferrihydrite, goethite, and lepidocrocite under neutral pH conditions. *Appl. Geochem.* **2013**, *28*, 185–193. [CrossRef]

36. Lee, H.; Kim, D.; Kim, J.; MinKyu, J.; Han, Y.S.; Park, Y.T.; Yun, H.S.; Choi, J. As (III) and As (V) removal from the aqueous phase via adsorption onto acid mine drainage sludge (AMDS) alginate beads and goethite alginate beads. *J. Hazard. Mater.* **2015**, *292*, 146–154. [CrossRef] [PubMed]

37. Asta, M.P.; Cama, J.; Martínez, M.; Giménez, J. Arsenic removal by goethite and jarosite in acidic conditions and its environmental implications. *J. Hazard. Mater.* **2009**, *171*, 965–972. [CrossRef]

38. Shih, Y.J.; Huang, R.L.; Huang, Y.H. Adsorptive removal of arsenic using a novel akhtenskite coated waste goethite. *J. Clean. Prod.* **2015**, *87*, 897–905. [CrossRef]

39. Rovira, M.; Gimenez, J.; Martınez, M.; Martınez-Llado, X.; de Pablo, J.; Mart, V.; Duro, L. Sorption of selenium (IV) and selenium (VI) onto natural iron oxides: Goethite and hematite. *J. Hazard. Mater* **2008**, *150*, 279–284. [CrossRef]

40. Zelmanov, G.; Semiat, R. Selenium removal from water and its recovery using iron (Fe^{3+}) oxide/hydroxide-based nanoparticles sol (NanoFe) as an adsorbent. *Sep. Purif. Technol.* **2013**, *103*, 167–172. [CrossRef]

41. Peak, D.; Sparks, D.L. Mechanisms of Selenate Adsorption on Iron Oxides and Hydroxides. *Environ. Sci. Technol.* **2002**, *36*, 1460–1466. [CrossRef]

42. Dichiara, A.B.; Webber, M.R.; Gorman, W.R.; Rogers, R.E. Removal of copper ions from aqueous solutions via adsorption on carbon nanocomposites. *ACS Appl. Mater. Interfaces* **2015**, *7*, 15674–15680. [CrossRef]

43. Jacobson, A.T.; Fan, M. Evaluation of natural goethite on the removal of arsenate and selenite from water. *J. Environ. Sci.* **2019**, *76*, 133–141. [CrossRef] [PubMed]

44. Matulová, M.; Bujdoš, M.; Miglierini, M.B.; Mitróová, Z.; Kubovčíková, U.M. The effects of selenate on goethite synthesis and selenate sorption kinetics onto a goethite surface-A three-step process with an unexpected desorption phase. *Chem. Geol.* **2020**, *556*, 119852. [CrossRef]

45. Balistrieri, L.S.; Chao, T.T. Selenium adsorption by goethite. *Soil Sci. Soc. Am. J.* **1987**, *51*, 1145–1151. [CrossRef]

46. Hayes, K.F.; Roe, A.L.; Brown Jr, G.A.; Hodgson, K.O.; Leckie, J.O.; Parks, G.A. In situ X-ray absorption study of surface complexes: Selenium oxyanions on α-FeOOH. *Science* **1987**, *238*, 783–786. [CrossRef]

47. Duc, M.; Lefevre, G.; Fedoroff, M.; Jeanjean, J.; Rouchaud, J.C.; Monteil-Rivera, F.; Milonjic, S. Sorption of selenium anionic species on apatites and iron oxides from aqueous solutions. *J. Environ. Radioact.* **2003**, *70*, 61–72. [CrossRef]

48. Wijnja, H.; Schulthess, C.P. Vibrational spectroscopy study of selenate and sulfate adsorption mechanisms on Fe and Al (hydr) oxide surfaces. *J. Colloid Interface Sci.* **2000**, *229*, 286–297. [CrossRef] [PubMed]

49. Jadhav, A.S.; Amrani, M.A.; Singh, S.K.; Al-Fatesh, A.S.; Bansiwal, A.; Srikanth, V.V.; Labhasetwar, N.K. γ-FeOOH and γ-FeOOH decorated multi-layer graphene: Potential materials for selenium (VI) removal from water. *J. Water Process Eng.* **2020**, *37*, 101396. [CrossRef]

Publisher's Note: MDPI stays neutral with regard to jurisdictional claims in published maps and institutional affiliations.